Structural Chemistry (2019) 30:1173–1184
https://doi.org/10.1007/s11224-018-1259-1

ORIGINAL RESEARCH

# Theoretical study on the [4+2] cycloaddition of 1,3-dimethylindole with 2,6-dimethylquinone

Mousa Soleymani [1]

Received: 31 October 2018 / Accepted: 4 December 2018 / Published online: 8 January 2019


## Abstract

The [4+2] cycloaddition reaction of 1,3-dimethylindole and *ortho*-quinone methide (obtained from tautomerization of 2,6-dimethylquinone under basic conditions), experimentally studied by Wen and co-workers, was theoretically studied at the B3LYP/6-311G** and M062X/6-311G** computational levels in both gas and ethanol solution phases. Two possible reactive channels were considered between the reactants and their theoretical parameters were calculated. The results indicated that the formation of the experimentally reported product is clearly confirmed by the analysis of the calculated Fukui and Parr functions reactivity indices. Transition states analysis showed that the experimentally reported product is both kinetically and thermodynamically preferred than the other regioisomeric adduct. The intrinsic reaction coordinates analysis indicated that in contrast to the proposed stepwise mechanism by Wen and co-workers, the reaction proceeds in one step without formation of any stable intermediate. Analysis of the global electron density transfer (GEDT) showed that the corresponding transition state is relatively polar and the electron density is fluxed from 1,3-dimethylindole toward *ortho*-quinone methide. Because of the polar character of the transition state, the reaction accelerates in ethanol, as a polar solvent, in comparison to the gas phase. Analysis of the frontier molecular orbitals showed that the HOMO orbital of 1,3-dimethylindole as a donor is also the frontier effective-for-reaction molecular orbital (FERMO). According to the Wiberg bond indexes and atoms in molecules analysis, it was found that both reactive channels take place via an asynchronous concerted mechanism.

**Keywords** Polycyclic indoline · 1,3-Dimethylindole · *ortho*-Quinone methide · DFT · FERMO · Local reactivity

## Introduction

A reaction in which two molecules combine to produce a cyclic adduct is known as cycloaddition. The [4+2] cycloaddition, known also as Diels-Alder reaction, is one of the most well-known and useful reactions, and is extensively used in chemistry. This reaction takes place when a four-atom component, namely diene, is attacked by an unsaturated bond, namely dienophile, to generate a six-membered homocyclic and heterocyclic compounds usually in a highly regio- and stereoselective fashion [1]. In the transition state relevant to the Diels-Alder reaction, the diene and dienophile approach together in approximately parallel planes. For most systems, the experimental and theoretical studies are in agreement with a concerted mechanism [2]. It has been found that in a reaction that involves unsymmetrical diene and dienophiles, the degree of advancement of bond formation might be different at one pair of termini than that at the other. This situation is indicative of a stepwise asynchronous mechanism along with formation of a zwitterionic intermediate [3]. Usually, the reaction between dienes and dienophiles with a very different electronic character takes place via a stepwise asynchronous mechanism. Alternatively, in some cases which the first single bond is formed between the diene and the dienophile in the rate-determining step, the second bond is barely beginning to form in the transition state. This two-stage mechanism is known as an asynchronous concerted one according to Houk's definition, in which the formation of two bonds takes place in separate, but overlapping, processes [4].

The solvent plays an important role on the rate of Diels-Alder reactions. In many cases, the rate and mechanism of reaction are sensitive to solvent polarity. For instance, water and other highly polar solvents enhance the rate of some

**Electronic supplementary material** The online version of this article (https://doi.org/10.1007/s11224-018-1259-1) contains supplementary material, which is available to authorized users.

✉ Mousa Soleymani
m.soleymani@abru.ac.ir; m_soleymani2007@yahoo.com

[1] Department of Chemistry, Faculty of Science, University of Ayatollah Alozma Borujerdi, Borujerd 6919969411, Iran

Diels-Alder reactions [5–7]. The "enforced hydrophobic interaction" effect is responsible of the accelerating effect of water, in which the strong hydrogen bonding network in water causes to exclude non-polar reactants and closes them together, resulting in the increase of effective concentrations [8]. In some cases, more solvation and consequently more stabilization of transition states than the reactants can contribute to the rate acceleration [9].

Polycyclic indolines, which are one class of nitrogen-containing heterocycles, have received considerable attention because of their ubiquitous presence in natural products and biologically active compounds [10–12]. It has proven that certain compounds containing a quinoline-fused indoline core exhibit anticancer and insecticidal activities [13, 14]. Due to various pharmacological activities, the development of efficient synthetic protocols to build such polyheterocyclic skeletons is of interest and many organic researchers have focused their attention on the synthesis of indole alkaloids [15, 16].

In 2017, Wen et al. reported an intermolecular [4+2] cycloaddition reaction between 2,6-dimethylquinone **1a** and 1,3-disubstituted indoles **2** in basic conditions for the synthesis of polycyclic indolines **3** (Scheme 1) [17].

The proposed mechanism includes the initial tautomerization of 2,6-dimethylquinone **1a** under basic conditions which leads to the formation of *ortho*-quinone methide **QM**. Nucleophilic attack of 1,3-disubstituted indoles on *ortho*-quinone methide **QM** generates a zwitterionic intermediate which undergoes a ring closure to afford corresponding polycyclic indoline **3** (Scheme 2).

Since reliable theoretical studies can support the experimental outcomes, we have investigated theoretically the [4+2] cycloaddition reactions of 1,3-dimethylindoles and 2,6-dimethylquinone by computational methods in continuous of our previous theoretical studies on various organic compounds [18–21]. The important aims of this work are as follows:

- Analysis of global and local reactivity indices at the ground state of the reagents involved in the Diels-Alder reaction of 1,3-dimethylindole toward *ortho*-quinone methide **QM**.
- To elucidate the kinetic and thermodynamic aspects of the reaction.
- To study the regioselectivity of the reaction.
- Determination of solvation effects on the reaction mechanism.
- To study the charge transfer at transition states.
- To study the bond formation and structural changes during the reaction using atoms in molecules (AIM) analysis.
- Investigation of the reaction synchronicity.

## Results and discussion

### Analysis of the global reactivity indices of the reactants

Global reactivity indices, namely chemical potential ($\mu$), chemical hardness ($\eta$), global electrophilicity ($\omega$), and global nucleophilicity ($N$), are one of the important tools to elucidate the reactivity of the reactants and regioselectivity in the cycloaddition reactions [22, 23]. Also, based on the model established by Domingo and co-workers, the polar or non-polar character of a reaction can be evaluated using analysis of the reactivity indices [24]. Thus, to study the reactivity of the reactants and polar character of the reaction, the global reactivity indices were calculated for *ortho*-quinone methide **QM** and 1,3-dimethylindole (**2a**, $R^1 = H$, $R^2 = R^3 = Me$) in both gas and ethanol phases which are given in Table 1.

A comparison of the results presented in Table 1 reveals that the electronic chemical potential of **2a** is higher than that of **QM**, which is indicative of fluxing the electron density from **2a** toward **QM** along the corresponding cycloaddition reaction. Also, the calculated values of the nucleophilicity $N$ and electrophilicity $\omega$

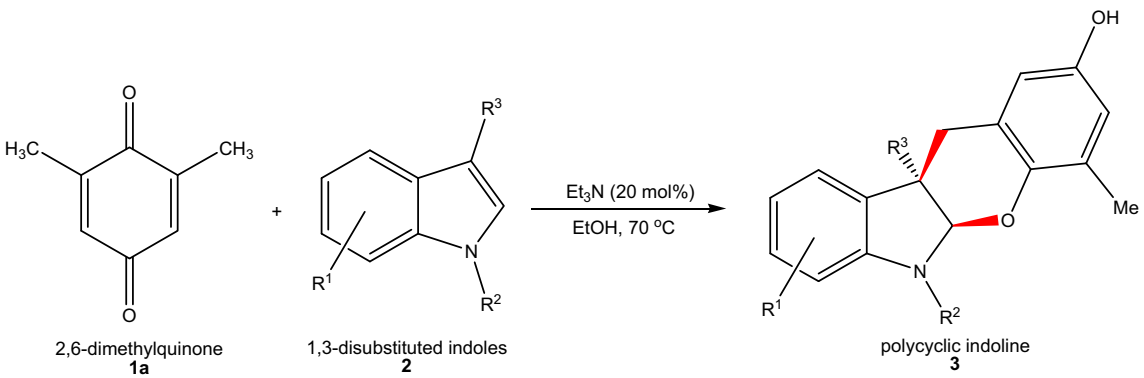


**Scheme 1** Synthesis of polycyclic indolines through [4+2] cycloaddition reaction

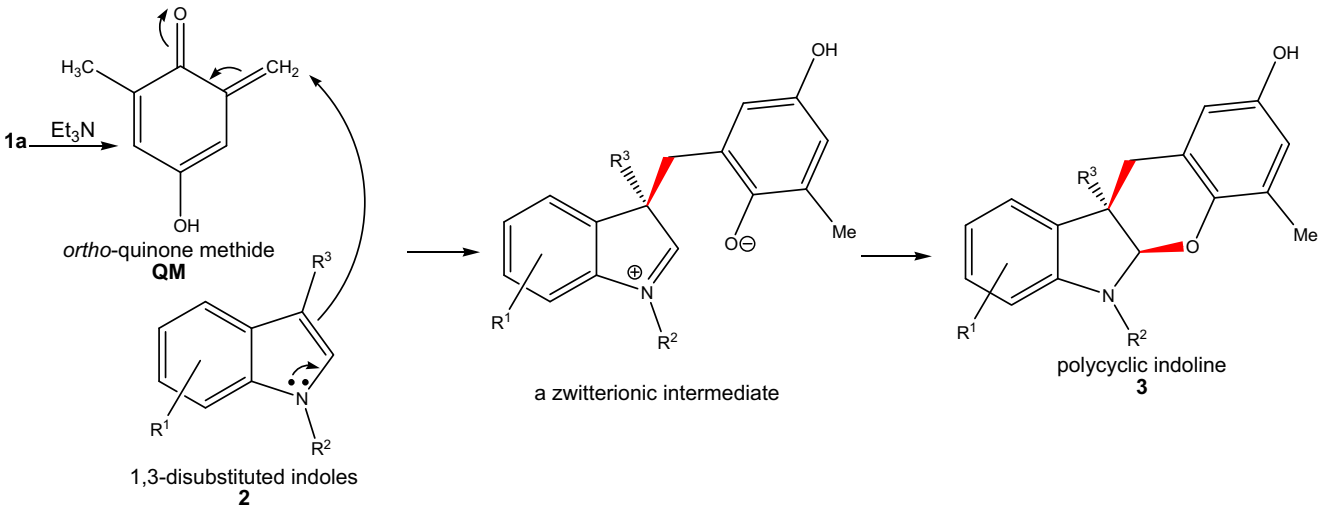


**Scheme 2** The proposed mechanism for the synthesis of polycyclic indolines via cycloaddition reaction between 1,3-disubstituted indoles and 2,6-dimethylquinone

indices identify that **QM** and **2a** being classified as a strong electrophile and strong nucleophile, respectively. According to Domingo's model, the polar character of the reactions can be evaluated using calculation of $\Delta\omega$ between the reagents [24]. High values of $\Delta\omega$ predict fast reactions between the reactants due to the low barriers. In the gas phase, the value of $\Delta\omega$, 4.18 (for B3LYP/6-311G** method) and 2.33 (for M062X/6-311G** method), predicts a high polar reaction between **QM** and **2a**. The same trend is also observed in the solution phase in which a large value of $\Delta\omega$ is obtained by using two computational methods (4.24 for B3LYP/6-311G** and 2.32 for M062X/6-311G** method).

## Study of the regioselectivity of the reaction

To study the regioselectivity in the title reaction, two possible reactive channels were considered between the reactants, **QM** and **2a**, in which they are added together to generate two regioisomeric adducts **3a** and **3a′** (Scheme 3). In the first reactive channels, the $C_\theta$ and $C_\phi$ atoms of **2a** interact respectively with $C_\delta$ and $O_\alpha$ atoms of **QM** to afford the corresponding cycloadduct **3a**. Alternatively, another regioisomer, **3a′**, is formed when $C_\theta$ and $C_\phi$ atoms of **2a** interact respectively with $O_\alpha$ and $C_\delta$ atoms of **QM** during the second reactive channel. As discussed in the "Introduction" section, Wen et al. reported experimentally the regioselective formation of the **3a** adduct from cycloaddition reaction between **QM** and **2a** [17].

**Table 1** The B3LYP/6-311G** and M062X/6-311G** computed electronic chemical potential ($\mu$), chemical hardness ($\eta$), and global nucleophilicity ($N$), in *eV*, for **QM** and **2a** in both gas and ethanol phases

| Species | B3LYP/6-311G** | | | | M062X/6-311G** | | | |
|---|---|---|---|---|---|---|---|---|
| | $\mu$ | $\eta$ | $N$ | $\omega$ | $\mu$ | $\eta$ | $N$ | $\omega$ |
| **QM** (gas) | −4.28 | 1.58 | 3.52 | 5.80 | −4.43 | 2.72 | 3.68 | 3.60 |
| **QM** (EtOH) | −4.36 | 1.55 | 3.07 | 6.11 | −4.53 | 2.70 | 3.23 | 3.79 |
| **2a** (gas) | −2.86 | 2.52 | 3.99 | 1.62 | −3.03 | 3.61 | 4.18 | 1.27 |
| **2a** (EtOH) | −3.06 | 2.50 | 3.43 | 1.87 | −3.25 | 3.59 | 3.61 | 1.47 |

When a non-symmetric nucleophile/electrophile pair approaches together, the most probable event is that the most nucleophilic center of nucleophile interacts with the most electrophilic center of electrophile. The Fukui functions reactivity indices are one of the powerful tools to study the reactivity of the reactants and regioselectivity. In 1984, Yang and Mortier introduced an approach to calculate the Fukui functions using the variation of the Mulliken population of an atom, $q_k$, which undergoes electrophilic or nucleophilic attack [25]:

$$f_k^- = q_k(N) - q_k(N-1) \quad \text{for electrophilic attacks}$$
$$f_k^+ = q_k(N+1) - q_k(N) \quad \text{for nucleophilic attacks}$$

the local electrophilicity $\omega_k$ and local nucleophilicity $N_k$ are calculated from the following equations where $\omega$ and $N$ refer to the global electrophilicity and nucleophilicity indices, respectively [26, 27]:

$$\omega_k = \omega f_k^+$$
$$N_k = N f_k^-$$

The local reactivity indices, $\omega_k$ and $N_k$, can be used satisfactorily to explain the reactivity and regioselectivity in various polar cycloadditions.

To investigate the observed regioselectivity in the reaction between **2a** and **QM** which is responsible for the formation of **3a** adduct [17], the local electrophilicity and nucleophilicity indices were calculated using NBO and Hirshfeld and Mulliken population analyses. Since, in this reaction **2a** acts as the nucleophile and **QM** acts as the electrophile, the local nucleophilicity

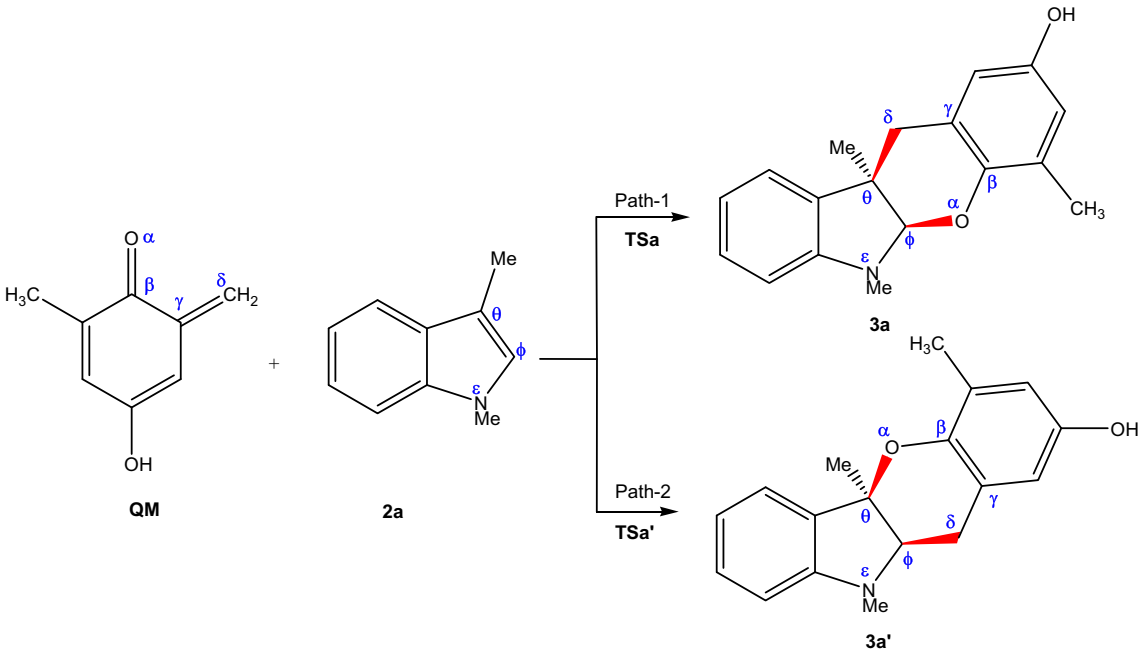


**Scheme 3** Two possible reactive channels between **QM** and **2a**

($N_k$) of **2a** and local electrophilicity ($\omega_k$) of **QM** were calculated. The results are given in Table 2.

Analysis of the local Fukui functions presented in Table 2 indicates that **QM** is more electrophilically activated at the δ-carbon atom. On the other hand, in contrast to the Mulliken analysis, the NBO and Hirshfeld ones indicate that **2a** is more nucleophilically activated at the θ-carbon atom than the ϕ-carbon atom. Accordingly, it is proposed that the most favorable nucleophile-electrophile interaction along the nucleophilic attack of **2a** on **QM** will take place between the δ-carbon atom as the most electrophilic center of **QM** and the θ-carbon atom as the most nucleophilic center of **2a**. This interaction leads to the formation of **3a** cycloadduct which is excellently consistent with the experimental reports, because this cycloadduct is the regiospecific product for the title reaction [17]. It is noteworthy that the Mulliken population analysis fails to explain regioselective formation of **3a** adduct, because the corresponding results indicate that **2a** is more nucleophilically activated at the ϕ-carbon atom. Thus, the corresponding interaction leads to the formation of **3a′** adduct.

An alternative way to study the local reactivity and regioselectivity in polar reactions is based on nucleophilic $P_k^-$ and electrophilic $P_k^+$ Parr functions which was recently introduced by Domingo and co-workers [28, 29]. Parr functions are obtained in terms of the variations of spin electron density that originate from electron transfer processes in polar reactions. As mentioned above, the compound **2a** acts as the nucleophile (toward **QM**); therefore, the $P_k^-$ Parr functions of **2a** and $P_k^+$ of **QM** were calculated. Table 3 summarizes the calculated Parr functions of **2a** and **QM** molecules.

Analysis of the calculated nucleophilic and electrophilic Parr functions presented in Table 3 designates that both Mulliken and Hirshfeld analyses can satisfactorily explain

**Table 2** The calculated values of the local electrophilicity and nucleophilicity obtained from NBO and Hirshfeld and Mulliken population analyses

| Analysis | Local electrophilicity (**QM**) | | | | Local nucleophilicity (**2a**) | | |
|---|---|---|---|---|---|---|---|
| | $\omega_\alpha$ | $\omega_\beta$ | $\omega_\gamma$ | $\omega_\delta$ | $N_\theta$ | $N_\phi$ | $N_\varepsilon$ |
| Mulliken[a] | 0.687 | 0.381 | −0.206 | 0.807 | 0.092 | 0.128 | 0.077 |
| NBO[a] | 0.835 | 0.464 | −0.029 | 1.311 | 0.324 | 0.106 | 0.198 |
| Hirshfeld[a] | 0.698 | 0.461 | 0.236 | 0.834 | 0.175 | 0.131 | 0.127 |
| Mulliken[b] | 0.443 | 0.256 | −0.204 | 0.603 | 0.094 | 0.112 | 0.067 |
| NBO[b] | 0.536 | 0.317 | −0.050 | 0.853 | 0.295 | 0.084 | 0.165 |
| Hirshfeld[b] | 0.448 | 0.302 | 0.138 | 0.531 | 0.154 | 0.108 | 0.104 |

[a] Obtained from B3LYP/6-311G** method

[b] Obtained from M062X/6-311G** method

**Table 3** The calculated values of the nucleophilic $P_k^-$ and electrophilic $P_k^+$ Parr functions of the **2a** and **QM** molecules

| Analysis | Electrophilic Parr functions | | | | Nucleophilic Parr functions | | |
|---|---|---|---|---|---|---|---|
| | $P_\alpha^+$ | $P_\beta^+$ | $P_\gamma^+$ | $P_\delta^+$ | $P_\theta^-$ | $P_\phi^-$ | $P_\varepsilon^-$ |
| Mulliken[a] | 0.160 | 0.118 | −0.107 | 0.482 | 0.376 | 0.034 | 0.252 |
| Hirshfeld[a] | 0.150 | 0.114 | 0.011 | 0.297 | 0.243 | 0.087 | 0.198 |
| Mulliken[b] | 0.180 | 0.119 | −0.114 | 0.457 | 0.422 | 0.042 | 0.262 |
| Hirshfeld[b] | 0.170 | 0.116 | 0.014 | 0.273 | 0.269 | 0.100 | 0.205 |

[a] Obtained from B3LYP/6-311G** method

[b] Obtained from M062X/6-311G** method

the formation of **3a** adduct. It is noteworthy that the most nucleophilic/electrophilic interaction takes place between the δ-carbon as the most electrophilic site of **QM** and the θ-carbon atom as the most nucleophilic center of **2a** which leads to the formation of **3a** adduct. So again, the electrophilic and nucleophilic Parr functions give a satisfactory description about the σ-bond formation between **QM** and **2a** fragments.

As an attempt to test the aforementioned local reactivity indices and also to study the regioselectivity, the transition states associated with the two reactive channels between **QM** and **2a** were calculated and detected by using two computational methods. Analysis of the intrinsic reaction coordinates (IRC) profiles associated with the two transition states involved in two reactive channels between **QM** and **2a** evidently revealed that formation of the corresponding cycloadducts **3a** as well as **3a′** takes place via a one-step mechanism without generation of any stable intermediate. While Wen et al. believe that the reaction takes place via a stepwise mechanism along with generation of a zwitterionic intermediate (Scheme 2) [17], the IRC analysis ruled out the formation of any stable intermediate in both gas and solution phases.

In order to compare two reactive channels from an energy viewpoint, the thermodynamic and kinetic parameters were calculated from optimized geometries of the reactants, transition states, and products. Table 4 gives the calculated results in both gas and ethanol phases obtained from M062X/6-311G** method. Also, the results obtained from B3LYP/6-311G** method are given in Table S1 of the supporting information.

In order to portray the energetic aspects of the studied reactive channels in a more evident and comparable manner, the corresponding free energies diagrams were plotted for both gas and solution phases which are depicted in Fig. 1.

Analysis of the results presented in Table 4 and Fig. 1 indicates that:

(a) Both reactive channels are possible thermodynamically because the corresponding products lie lower than the reactants. According to kinetic principles, the rate of **3a** and **3a′** formation can be considered as $k$[**2a**][**QM**] and $k'$[**2a**][**QM**], respectively, where $k$ and $k'$ are the second-order rate constants. Consequently, the concentration ratio of **3a** to **3a′** in the reaction mixture becomes:

$$\frac{[\mathbf{3a}]}{[\mathbf{3a}']} = \frac{k}{k'}$$

according to the Eyring equation, the rate constant is defined as:

$$k = \left(\frac{K_B T}{h}\right) \exp\left(\frac{-\Delta G^{\ddagger}}{RT}\right)$$

where $K_B$ is the Boltzmann constant, $h$ is Plank's constant, $T$ is the Kelvin temperature, $\Delta G^{\ddagger}$ is the Gibbs free energy of activation, and $R$ is the universal gas constant [30].

Thus, it can be concluded that:

$$\frac{[\mathbf{3a}]}{[\mathbf{3a}']} = \exp\left(\frac{\Delta G^{\ddagger\prime} - \Delta G^{\ddagger}}{RT}\right)$$

The calculated values of $\Delta G^{\ddagger}$ and $\Delta G^{\ddagger\prime}$ at the solution phase are 81.13 and 95.31 kJ mol$^{-1}$, respectively, and the $\frac{[\mathbf{3a}]}{[\mathbf{3a}']}$ ratio turn into 305.0. Accordingly, the percentage of **3a** becomes 99.66% which indicates that is approximately the only product present in the reaction mixture and the title cycloaddition reaction takes place via a stereospecific fashion to generate **3a**.

(b) The reactive channel 1 is more kinetically and themodynamically favored than the reactive channel 2 which is consistent with the experimental outcomes [17]. The reactive channel 1 produces **3a** adduct with a rate constant of

**Table 4** Calculated enthalpies ($H$, in au), entropies ($S$, in J mol$^{-1}$ K$^{-1}$), Gibbs free energies ($G$, in au), relative enthalpies ($\Delta H$, in kJ mol$^{-1}$), entropies ($\Delta S$ in J mol$^{-1}$ K$^{-1}$), Gibbs free energies ($\Delta G$, in kJ mol$^{-1}$), and the reaction rate constant ($k$, in s$^{-1}$) for the reactions of **QM** and **2a** in the gas and ethanol phases obtained from M062X/6-311G** method. The calculated parameters corresponding to the solution phase are given in parentheses

| | $H$ | $\Delta H$ | $G$ | $\Delta G$ | $S$ | $\Delta S$ | $k$ |
|---|---|---|---|---|---|---|---|
| **QM** | −459.8498 (−459.8604) | – | −459.8947 (−459.9051) | – | 395.30 (393.99) | – | – |
| **2a** | −442.1613 (−442.1693) | – | −442.2077 (−442.2128) | – | 408.64 (382.90) | – | – |
| **TSa** | −902.0025 (−902.0194) | 22.59 (27.03) | −902.0692 (−902.0870) | 87.15 (81.13) | 587.76 (594.71) | −216.19 (−182.17) | $3.31 \times 10^{-3}$ ($3.77 \times 10^{-2}$) |
| **3a** | −902.0692 (−902.0814) | −152.55 (−135.73) | −902.1335 (−902.1457) | −81.67 (−72.97) | 566.52 (565.92) | −237.40 (−210.96) | – |
| **TSa′** | −901.9943 (−902.0143) | 44.10 (40.42) | −902.0611 (−902.0816) | 108.45 (95.31) | 588.27 (592.45) | −215.69 (−184.43) | $6.14 \times 10^{-7}$ ($1.23 \times 10^{-4}$) |
| **3a′** | −902.0631 (−902.0763) | −136.52 (−122.34) | −902.1277 (−902.1416) | −66.44 (−62.22) | 569.59 (575.03) | −234.35 (−201.88) | – |

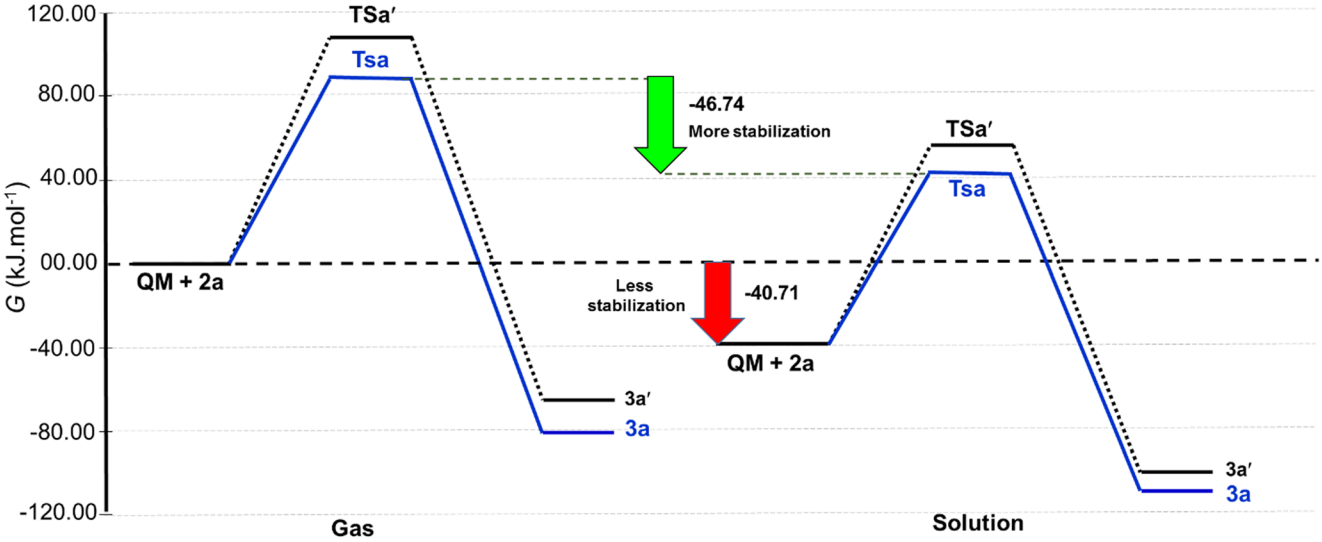


**Fig. 1** The free energy diagram for the reaction of **QM** and **2a** in the gas and ethanol phases obtained from M062X/6-311G** method

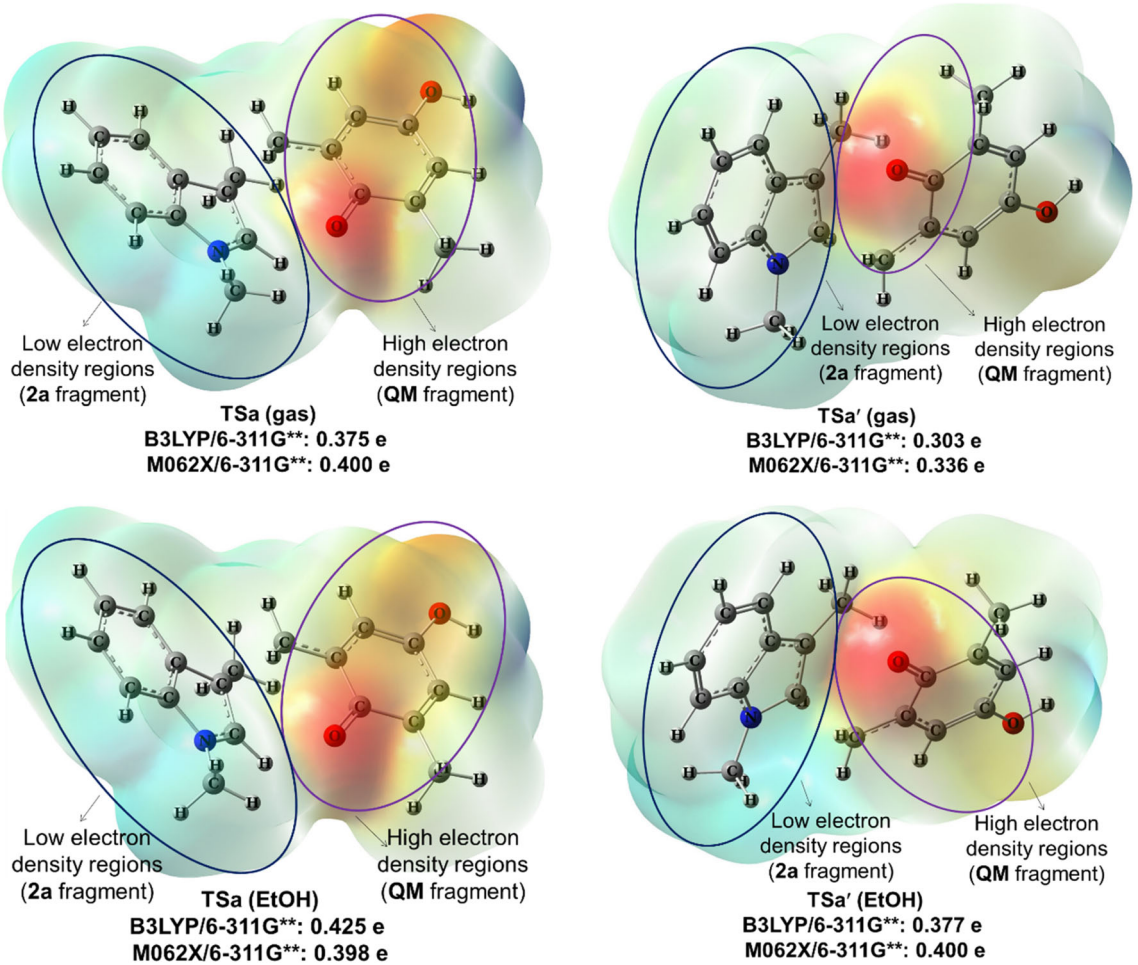


**Fig. 2** The molecular electrostatic potential maps and the global electron density transfer (GEDT) values obtained for **TSa** and **TSa′** in both gas and ethanol phases

$3.31 \times 10^{-3}$ $s^{-1}$ in the gas phase which is approximately 5400 times faster than the reactive channel 2 under the same conditions. Also, the first reactive channel proceeds with a rate constant of $3.77 \times 10^{-2}$ $s^{-1}$ in ethanol solution which is 300-fold higher than the second reactive channel. Thus, it can be concluded that ethanol as a polar solvent affects the reactive channel 2 more than the reactive channel 1.

(c) Generally, the polarity of the solvent, reactants, intermediates, and transition states plays an important role on the reactions rate. Since in the title reaction the transition states have more polar character compared to the reactants, the rate of the reactions is increased when they are carried out in ethanol with dielectric constant of 24.5. Ethanol as a polar solvent lowers the polar transition state energy level more than the reactants and decreases the activation energies.

(d) Because of the decreasing of the freedom degrees of the reactants along the reaction coordinate, the entropy of the reactions (ΔS) is decreased.

## Study of charge transfer in transition states

When an electrophilic/nucleophilic pair interacts together, the charge transfer can occur along the reaction and consequently, we deal with a polar reaction. Global electron density transfer (GEDT) can be considered as a relative criterion of charge transfer in transition states which is sometimes responsible for the barrier energies [31]. Therefore, to investigate the charge transfer associated with the reaction studied, the GEDT values were calculated for all transition states in both gas and ethanol phases. The molecular electrostatic potential (MESP) map of transition states was also obtained in order to portray the charge transfer in a better comparable manner. Figure 2 depicts the calculated values of GEDTs along with the MESP maps, which therein the red and blue colors represent respectively more negative (higher electron density) and more positive (lower electron density) regions.

Analysis of the GEDT values and MESP maps reveals that two reactive channels are polar and the electron density is fluxed from **2a** as nucleophile toward **QM** as electrophile. The red color in the molecular electrostatic map depicts the regions with high electron density around the α-oxygen atom of **QM** as electron acceptor. As said in the previous section, ethanol as a polar solvent affects the second reactive channel more than the first one, which can be attributed to this fact that the GEDT value of the reactive channel 2 increases more than the other, when going from the gas phase to the solution.

The changes in NBO atomic charges during the reaction were also calculated for both reactive channels. The results obtained from M062X/6-311G** method are given in Fig. 3 and those obtained from B3LYP/6-311G** method are given

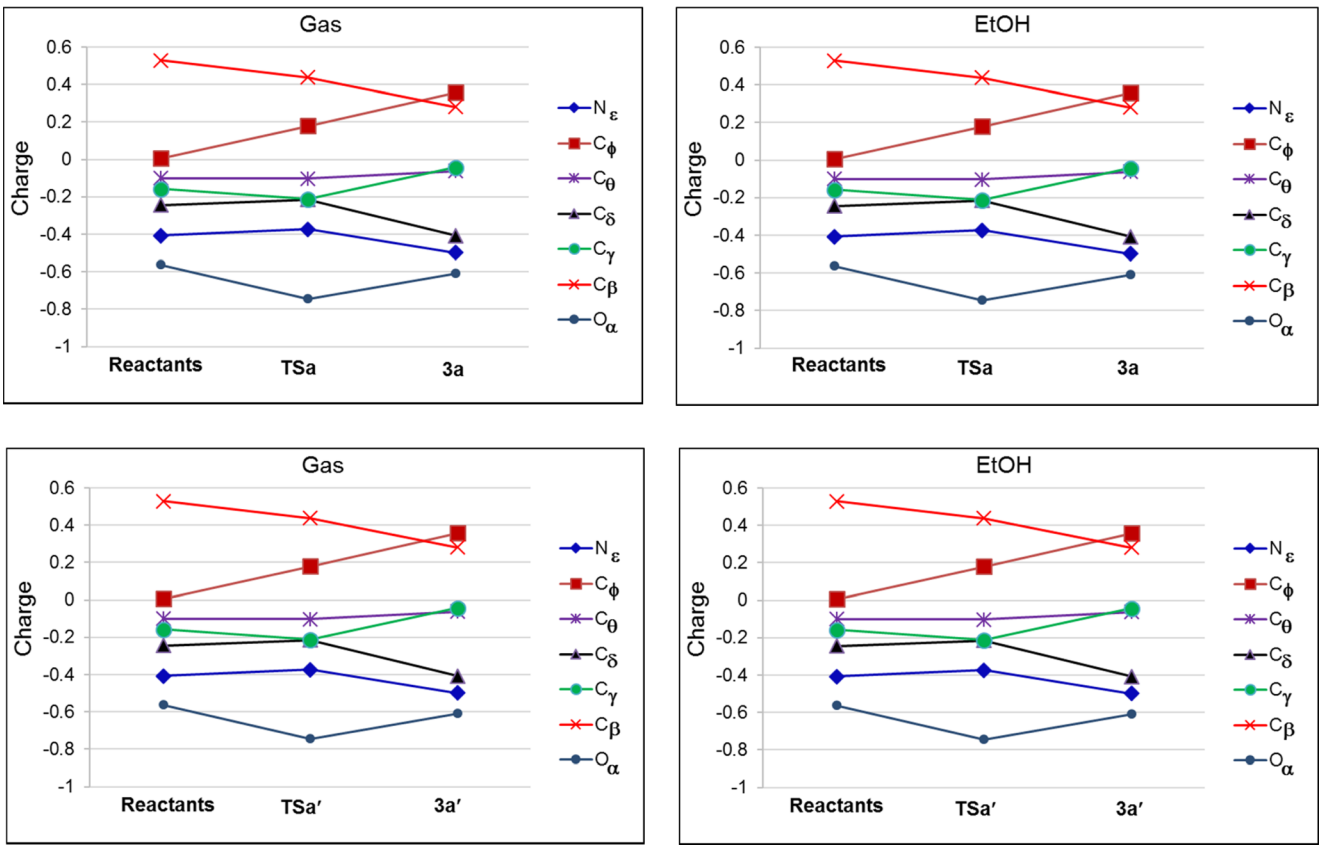


**Fig. 3** Changes in NBO atomic charges during the reaction of **2a** and **QM** obtained from M062X/6-311G** method

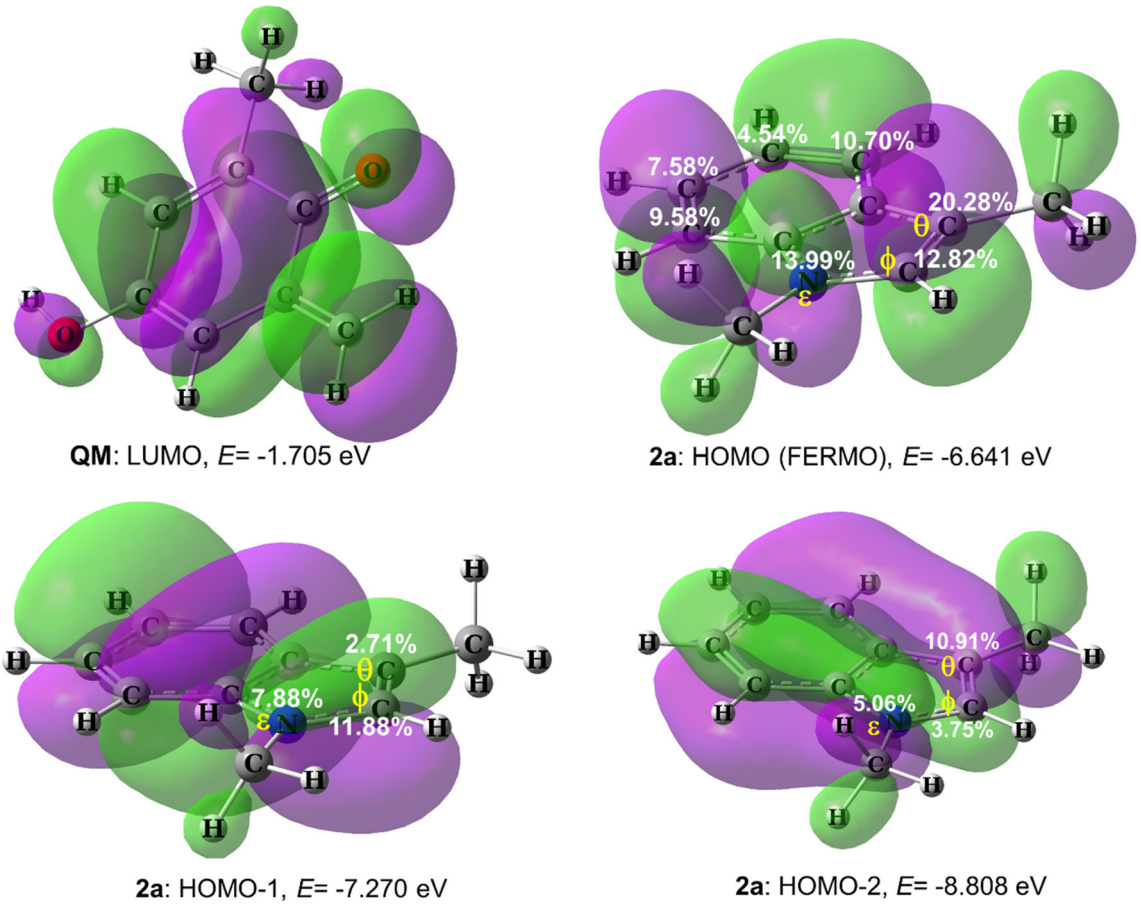


**Fig. 4** The LUMO of **QM** and the three highest occupied MOs of **2a** along with the relative contribution of the active sites

in Fig. S1 of supporting information. Because of electron transfer from **2a** toward **QM**, the charge of the ε, ϕ, and θ atoms (corresponding to **2a**) is increased in the transition states and that for the α, β, γ, and δ atoms (corresponding to **QM**) is decreased.

## Study of the interaction between frontier molecular orbitals of the reactants

Since, in the title reaction **QM** and **2a** respectively act as electron acceptor and donor, the interaction between the LUMO of the former and the HOMO of the later is concluded. Recently, the frontier effective-for-reaction molecular orbital (FERMO) concept has been introduced as a powerful approach to study the interaction between the frontier orbitals of the reactants. This theory considers the HOMO or an occupied molecular orbital close to the HOMO with large contribution of active sites. For many reactions, the FERMOs can work better than HOMO [32], because to determinate the interacting frontier orbitals, it considers both energy difference and contribution of active sites. We used satisfactorily the FERMO concept to describe the reactivity of the active sites of the pyrene [18]. Therefore, for determination of the FERMO of **2a** as the donor, the relative contribution of the active sites (θ, ϕ, and ε atoms) was calculated in the three highest occupied MOs. The results are given in Fig. 4. It is clear that in terms of the composition

**Table 5** The calculated values of synchronicity (Sy) for the reactions of **QM** with **2a** obtained from optimized structures using M062X/6-311G** method

| | | | | | | | | |
|---|---|---|---|---|---|---|---|---|
| Path-1 (gas) | $\delta B_{O\alpha\text{-}C\beta}$ | $\delta B_{C\beta\text{-}C\gamma}$ | $\delta B_{C\gamma\text{-}C\delta}$ | $\delta B_{C\delta\text{-}C\theta}$ | $\delta B_{C\theta\text{-}C\phi}$ | $\delta B_{C\phi\text{-}O\alpha}$ | $\delta B_{av}$ | $Sy$ |
| | 0.384 | 0.481 | 0.628 | 0.470 | 0.534 | 0.090 | 0.431 | 0.820 |
| Path-2 (gas) | $\delta B_{O\alpha\text{-}C\beta}$ | $\delta B_{C\beta\text{-}C\gamma}$ | $\delta B_{C\gamma\text{-}C\delta}$ | $\delta B_{C\delta\text{-}C\phi}$ | $\delta B_{C\theta\text{-}C\phi}$ | $\delta B_{C\theta\text{-}O\alpha}$ | $\delta B_{av}$ | $Sy$ |
| | 0.294 | 0.387 | 0.638 | 0.542 | 0.547 | 0.093 | 0.417 | 0.771 |
| Path-1 (EtOH) | $\delta B_{O\alpha\text{-}C\beta}$ | $\delta B_{C\beta\text{-}C\gamma}$ | $\delta B_{C\gamma\text{-}C\delta}$ | $\delta B_{C\delta\text{-}C\theta}$ | $\delta B_{C\theta\text{-}C\phi}$ | $\delta B_{C\phi\text{-}O\alpha}$ | $\delta B_{av}$ | $Sy$ |
| | 0.331 | 0.433 | 0.573 | 0.400 | 0.481 | 0.058 | 0.379 | 0.805 |
| Path-2 (EtOH) | $\delta B_{O\alpha\text{-}C\beta}$ | $\delta B_{C\beta\text{-}C\gamma}$ | $\delta B_{C\gamma\text{-}C\delta}$ | $\delta B_{C\delta\text{-}C\phi}$ | $\delta B_{C\theta\text{-}C\phi}$ | $\delta B_{C\theta\text{-}O\alpha}$ | $\delta B_{av}$ | $Sy$ |
| | 0.302 | 0.404 | 0.637 | 0.511 | 0.538 | 0.059 | 0.408 | 0.775 |

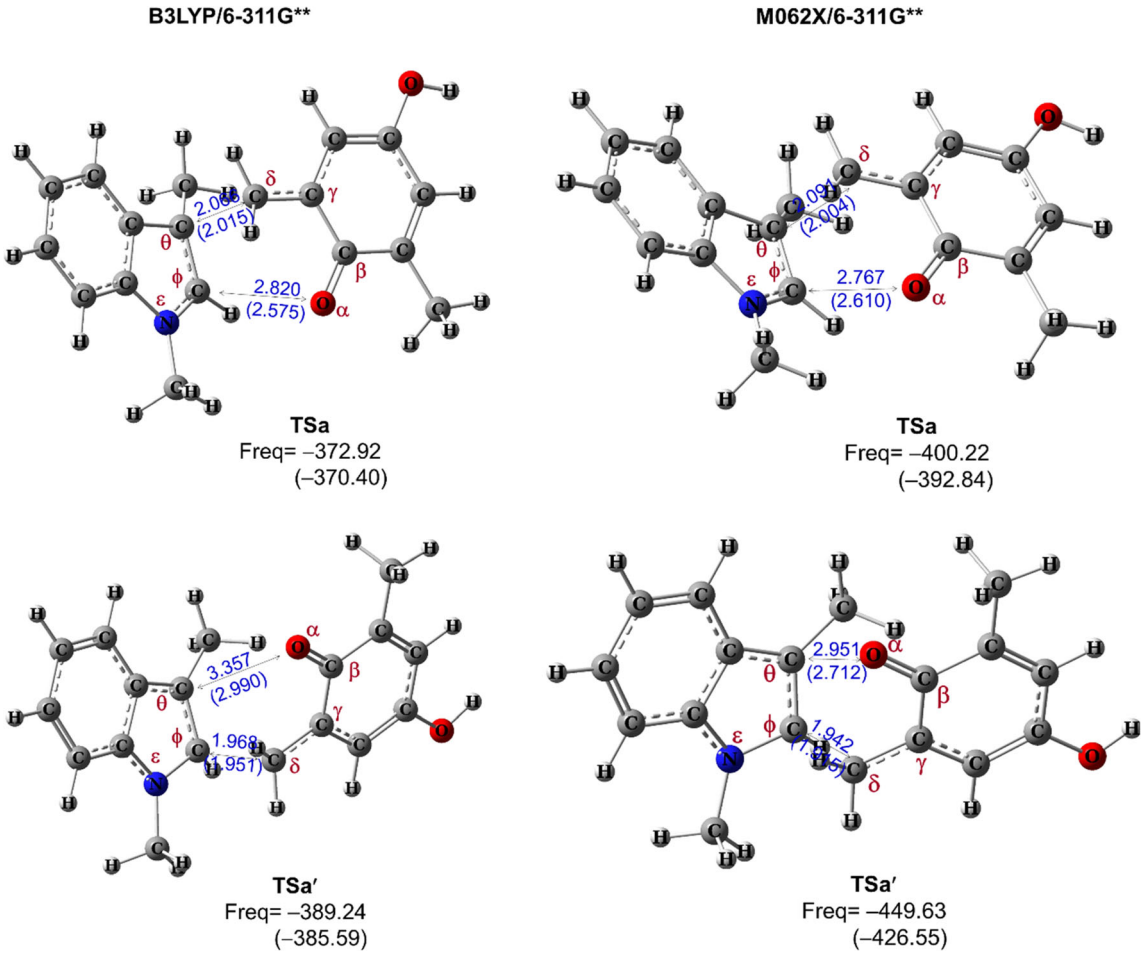


**Fig. 5** The optimized structure of the transition states in ethanol along with their imaginary frequencies as well as some bond lengths (Å). The results obtained in the gas phase are given in parenthesis

and location of the molecular orbitals, the FERMO is also the HOMO for the reaction, because the active sites of **2a** have a larger contribution in the HOMO in comparison to the other occupied MOs (13.99%, 12.82%, and 20.28%, respectively, for the ε, ϕ, and θ atoms). The larger contribution of the θ-carbon atom in the FERMO compared to the other active sites (ε, ϕ atoms) indicates that **2a** is activated nucleophilically at the θ-carbon atom, which is consistent with the local reactivity indices obtained from Fukui and Parr function analysis. On the other hand, analysis of the carbon atoms corresponding to the six-membered ring of **2a** indicates a lower contribution in FERMO and consequently lower reactivity compared to the five-membered ring atoms.

## Study of the synchronicity of the reactions

Cycloaddition reactions usually proceed via a synchronous mechanism in which the structural variations take place in

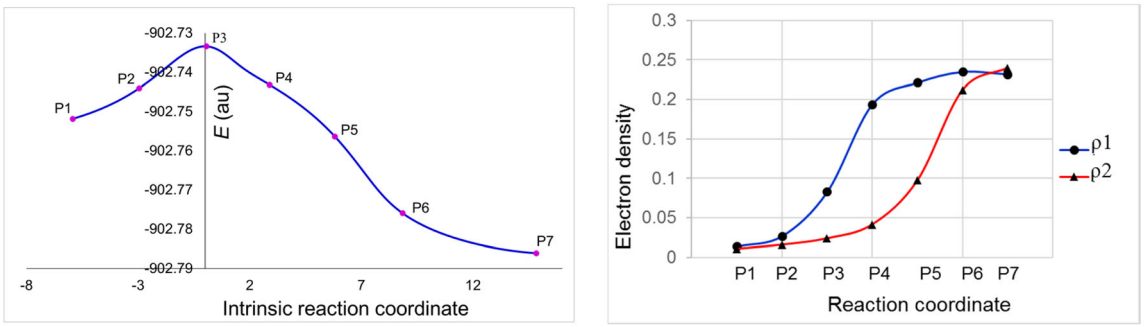


**Fig. 6** Intrinsic reaction coordinate (IRC) profile for the most preferred transition state (**TSa**) and the variations of BCP electron densities of $C_\theta$–$C_\delta$ ($\rho_1$) and $C_\phi$–$O_\alpha$ ($\rho_2$) bonds along the cycloaddition reaction of **QM** and **2a**

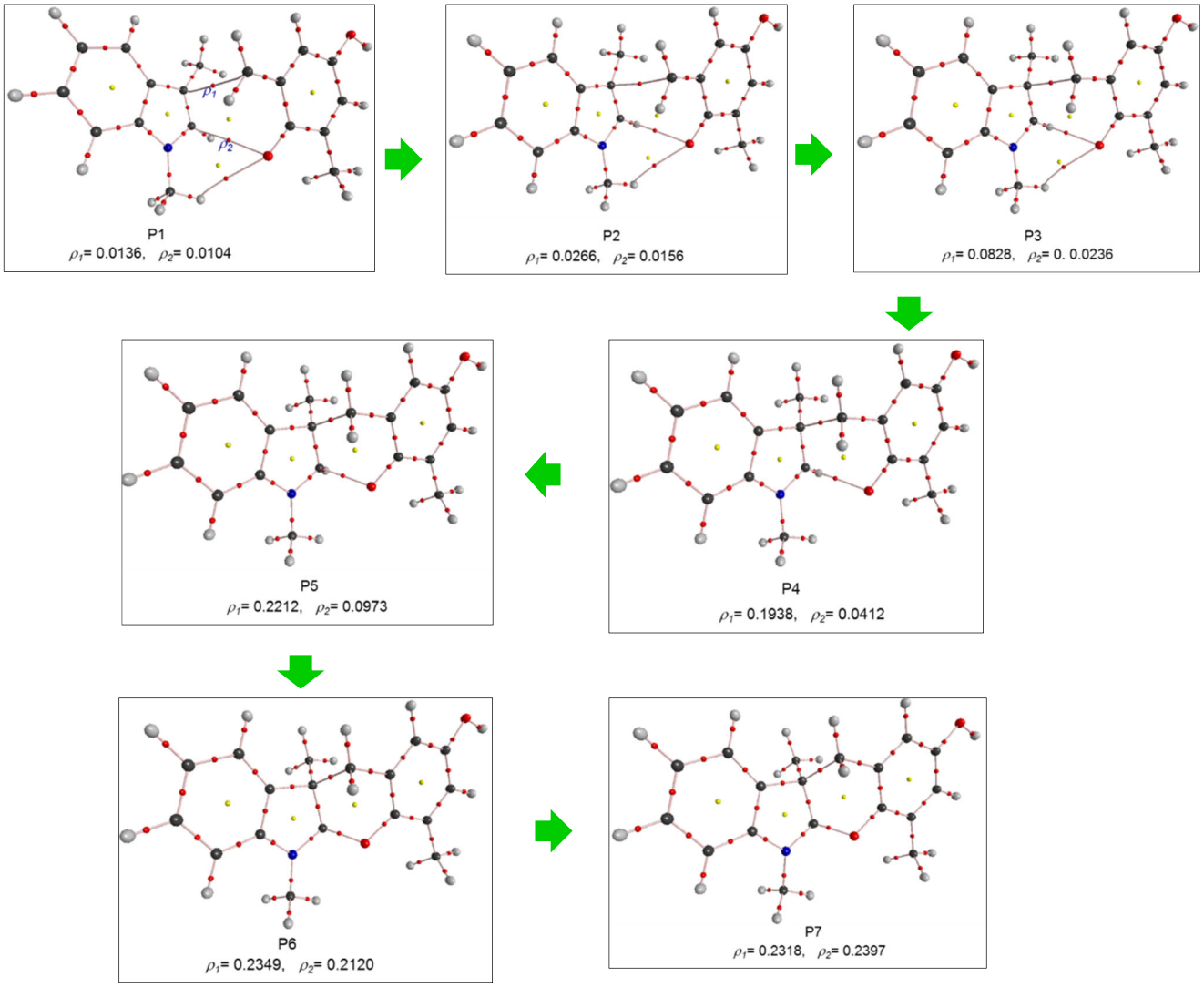


**Fig. 7** AIM topological analysis of $C_\theta$–$C_\delta$ and $C_\phi$–$O_\alpha$ single bond formation along the IRC profile of **TSa**

one step. Therefore, in order to understand the level of the synchronicity, the structural features of the transition states were studied by using Wiberg bond index analysis. Table 5 summarizes the calculated values of the synchronicity of both reactive channels under gas and solution conditions using M062X/6-311G** method. The results obtained from B3LYP/6-311G** are given in Table S2 of supporting information. Also, Fig. 5 depicts the optimized structure of the transition states along with their imaginary frequencies and the distances between interacting atoms of two fragments.

Analysis of the results presented in Table 5 reveals that both reactive channels are not completely synchronous. According to the bond distances presented in Fig. 5, the degree of advancement of the two new bonds between two fragments is not equivalent in the corresponding transition states. For instance, the bond lengths of $C_\theta$–$C_\delta$ and $C_\phi$–$C_\delta$ respectively in **TSa** and **TSa′** are less than those for $C_\phi$–$O_\alpha$ and $C_\theta$–$O_\alpha$ ones, respectively. Therefore, it can be said that the $C_\theta$–$C_\delta$ and $C_\varphi$–$C_\delta$ bonds in **TSa** and **TSa′**, respectively, are formed faster than the other bonds. This trend is completely consistent with the results of the local Fukui functions obtained from NBO and Hirshfeld analyses, because the most favorable interaction was found to be between the $C_\theta$ and $C_\delta$ atoms which results in **3a** adduct. A similar agreement is also observed for the reactive channel 2 between the Fukui function analysis and Wiberg bond indexes. Thus, the synchronicity and bond length analysis reveal that both cycloaddition channels take place via an asynchronous concerted mechanism.

## AIM study of the cycloaddition reaction of QM and 2a

AIM analysis is one of the suitable methods to study the structural changes during the cycloaddition reactions. Thus, the AIM analysis was performed along the IRC profile associated with the most preferred transition state, **TSa**. The molecular topological graphs and the electron densities ($\rho$) of the bond

critical points (BCP) corresponding to the two forming bonds, $C_\theta$–$C_\delta$ and $C_\phi$–$O_\alpha$, were obtained for certain points on the IRC profile. The variations of the BCP electron densities during the reaction coordinate were also obtained. The results are given in Figs. 6 and 7. At the first point associated with the IRC profile, P1, where the $C_\theta$–$C_\delta$ and $C_\phi$–$O_\alpha$ distances are 2.9081 and 2.9659 Å, respectively, two interacting moieties, **QM** and **2a**, are sufficiently far away from each other so that the corresponding BCP electron densities for $C_\theta$–$C_\delta$ and $C_\phi$–$O_\alpha$ bonds are relatively low ($\rho_1 = 0.0136$ and $\rho_2 = 0.0104$). When two reactants gradually approach each other, the BCP electron density for $C_\theta$–$C_\delta$ and $C_\phi$–$O_\alpha$ bonds is increased. For instance, the values of $\rho_1$ and $\rho_2$ in the transition state are 0.0828 and 0.0236, respectively. The increasing trend in the BCP electron densities continues to produce **3a** adduct at the P7 point, in which the $\rho_1$ and $\rho_2$ values reach to 0.2318 and 0.2397, respectively. A comparison of the variation of the BCP electron densities corresponding to the $C_\theta$–$C_\delta$ and $C_\phi$–$O_\alpha$ bonds presented in Fig. 6 indicates that the increasing trend of the electron density for the former bond is more than the later. Thus, it is concluded that the $C_\theta$–$C_\delta$ bond is formed faster than the $C_\phi$–$O_\alpha$ one, and consequently we deal with an asynchronous concerted cycloaddition reaction between **QM** and **2a**. These results indicate that the AIM analysis has satisfactory agreement with the Fukui function as well as synchronicity analysis.

## Conclusion

Computational methods at B3LYP/6-311G** and M062X/6-311G** levels of theory were applied to study [4+2] cycloaddition of 1,3-dimethylindole and *ortho*-quinone methide (obtained from tautomerization of 2,6-dimethylquinone) which was experimentally investigated by Wen et al. For this purpose, two possible reactive channels were considered between 1,3-dimethyindole and 2,6-dimethylquinone in both gas and ethanol solution which leads to generation of two possible regioisomeric adducts. Regioselective formation of the experimentally reported adduct was confirmed with Fukui function reactivity indices obtained from NBO and Hirshfeld analysis and also with the Parr functions reactivity indices obtained from Mulliken and Hirshfeld analyses. Transition state calculations confirmed that the reactive channel which generates the experimentally reported adduct is kinetically and thermodynamically the preferred path. Although Wen et al. believe that the reaction proceeds via a stepwise mechanism with formation of a zwitterionic intermediate, the IRC analysis ruled out the formation of any stable intermediate. For investigation of the charge transfer during the reaction, the global electron density transfer (GEDT) values were calculated for the transition states and the results indicated that all transition states are relatively polar in both gas and solution phases. Also, it was found that the electron density is fluxed from **2a** toward **QM**. AIM analysis and calculation of synchronicity revealed that all reactive channels proceed via an asynchronous concerted mechanism.

## Computational details

To study the cycloaddition reactions between 1,3-dimethylindole and *ortho*-quinone methide, the optimization of the reactants and products was carried out using B3LYP/6-311G** and M062X/6-311G methods [33, 34]. To calculate the solvation effects on the studied molecules, the conductor-like polarizable continuum model (CPCM) was used [35]. The structures of transition states were determined by using the Berny algorithm or the synchronous transit-guided quasi-Newton (STQN) procedure [36, 37]. The stationary points were characterized by frequency calculations to verify that all transition states have one and only one imaginary frequency. The accuracy of transition states was also verified by using IRC calculations [38, 39].

The atomic charges of the reactants, TS structures, and products were calculated using NBO analysis [40, 41].

The nucleophilicity index $N$ is defined as the following equation in which $E_{HOMO}(Nu)$, the HOMO energy of tetracyanoethylene (TCE), is taken as the reference and $E_{HOMO}(Nu)$ refers to the HOMO energy of nucleophile [42]:

$$N = E_{HOMO}(Nu) - E_{HOMO}(TCE)$$

The electrophilicity index $\omega$ is given by the following equation based on the chemical hardness $\eta$ and electronic chemical potential $\mu$ [43]. Both $\eta$ and $\mu$ quantities were calculated from the frontier molecular orbitals energies as $\mu \approx (E_{HOMO} + E_{LUMO})/2$ and $\eta \approx (E_{LUMO} - E_{HOMO})/2$ [44, 45].

$$\omega = \frac{\mu^2}{2\eta}$$

The synchronicity (Sy) in transition states was calculated with the following equation [46]:

$$S_y = 1 - \frac{1}{2n-2} \sum \frac{|\delta B_i - \delta B_{av}|}{\delta B_{av}}$$

where $n$ is the number of directly participating bonds in the reaction, $\delta B_i$ is a relative variation of bond index $B_i$ at the transition state, and $\delta B_{av}$ is a measure of the degree of advancement of the transition state along the reaction coordinate. The values of synchronicity vary from 0 for stepwise to 1 for concerted mechanisms.

All calculations were performed with the Gaussian 09 program package [47].

**Funding information** I am thankful to the Research Council and Office of Graduate Studies of the University of Ayatollah Alozma Borujerdi for their financial support.

## Compliance with ethical standards

**Conflict of interest** The author declares that he has no conflict of interest.

**Publisher's Note** Springer Nature remains neutral with regard to jurisdictional claims in published maps and institutional affiliations.

## References

1. Fringuelli F, Taticchi A (2002) The Diels-Alder reaction: selected practical methods. Wiley, Chichester
2. Gajewski JJ, Peterson KB, Kagel JR (1987). J Am Chem Soc 109: 5545–5546
3. Linder M, Brinck T (2012). J Org Chem 77:6563–6573
4. Houk KN, Gonzalez J, Li Y (1995). Acc Chem Res 28:81–90
5. Rideout D, Breslow R (1980). J Am Chem Soc 102:7816–7817
6. Breslow R, Guo T (1988). J Am Chem Soc 110:5613–5617
7. Dunams T, Hoekstra W, Pentaleri M, Liotta D (1988). Tetrahedron Lett 29:3745–3748
8. Otto S, Engberts JBFN (2000). Pure Appl Chem 72:1365–1372
9. Breslow R, Rizzo CJ (1991). J Am Chem Soc 113:4340–4341
10. Dewick PM (2002) Medicinal natural products: a biosynthetic approach2nd edn. Wiley, New York
11. Fattorusso E, Scafati OT (2008) Modern alkaloids. Wiley-VCH, Weinheim
12. Sanchis PR, Savina SA, Albericio F, Alvarez MA (2011). Chem Eur J 17:1388–1408
13. Trost BM, Osipov M (2015). Chem Eur J 21:16318–16343
14. Popov K, Hoang A, Somfai P (2016). Angew Chem Int Ed 55: 1801–1804
15. Yang J-M, Li P-H, Wei Y, Tang X-Y, Shi M (2016). Chem Commun 52:346–349
16. Cera G, Chiarucci M, Mazzanti A, Mancinelli M, Bandini M (2012). Org Lett 14:1350–1353
17. Lin Ch DH-J, Zhao H, Yan D-F, Liu N-X, Sun H, Wen X, Xu Q-L (2017). Org Biomol Chem 15:3472–3478
18. Soleymani M, Dashi Khavidaki H (2017). Comp Theor Chem 1112:37–45
19. Soleymani M (2018). Monatshe Chem Chem Mon 149:2183–2193
20. Memarian HR, Soleymani M, Sabzyan H, Bagherzadeh M, Ahmadi H (2011). J Phys Chem A 115:8264–8270
21. Memarian HR, Sabzyan H, Soleymani M, Habibi MH, Suzuki T (2011). J Mol Struc 998:91–98
22. Geerlings P, De Proft F, Langenaeker W (2003). Chem Rev 103: 1793–1874
23. Ess DH, Jones GO, Houk KN (2006). Adv Synth Catal 348:2337–2361
24. Domingo LR, Aurell MJ, Pérez P, Contreras R (2002). Tetrahedron 58:4417–4423
25. Yang W, Mortier WJ (1986). J Am Chem Soc 108:5708–5711
26. Domingo LR, Aurell MJ, Pêrez P, Contreras R (2002). J Phys Chem A 106:6871–6875
27. Pêrez P, Domingo LR, Duque-Noreňa M, Chamorro E (2009). J Mol Struct THEOCHEM 895:86–91
28. Domingo LR, Pérez P, Sáez JA (2013). RSC Adv 3:1486–1494
29. Chamorro E, Pérez P, Domingo LR (2013). Chem Phys Lett 582: 141–143
30. Eyring H (1935). J Chem Phys 3:107–115
31. Domingo LR (2014). RSC Adv 4:32415–32428
32. Da Silva RR, Ramalho TC, Santos JM, Figueroa-Villar JD (2006). J Phys Chem A 110:1031–1040
33. Lee C, Yang W, Parr RG (1988) Phys. Rev. B 37:785–789
34. Zhao Y, Truhlar DG (2006). J Phys Chem 110:5121–5129
35. Barone V, Cossi M (1998). J Phys Chem A 102:1995–2001
36. Schlegel HB (1982). J Comput Chem 3:214–218
37. Peng C, Ayala PY, Schlegel HB, Frisch MJ (1996). J Comput Chem 17:49–56
38. Gonzalez C, Schlegel HB (1989). J Chem Phys 90:2154–2161
39. Gonzalez C, Schlegel HB (1990). J Phys Chem 94:5523–5527
40. Reed AE, Curtiss LA, Weinhold F (1988). Chem Rev 88:899–926
41. Carpenter JE, Weinhold FJ (1988). J Mol Struct 169:41–62
42. Domingo LR, Perez P, Ortega DE (2013). J Org Chem 78:2462–2471
43. Parr RG, Szentpaly LV, Liu S (1999). J Am Chem Soc 121:1922–1924
44. Parr RG, Pearson RG (1983). J Am Chem Soc 105:7512–7516
45. Parr RG, Yang W (1989) Density functional theory of atoms and molecules. Oxford University Press, New York
46. Lecea B, Arrieta A, Roa G, Ugalde JM, Cossio FP (1994). J Am Chem Soc 116:9613–9619
47. Frisch MJ, Trucks GW, Schlegel HB, Scuseria GE, Robb MA, Cheeseman JR, Scalmani G, Barone V, Mennucci B, Petersson GA, Nakatsuji H, Caricato M, Li X, Hratchian HP, Izmaylov AF, Bloino J, Zheng G, Sonnenberg JL, Hada M, Ehara M, Toyota K, Fukuda R, Hasegawa J, Ishida M, Nakajima T, Honda Y, Kitao O, Nakai H, Vreven T, Montgomery JA, Peralta Jr JE, Ogliaro F, Bearpark M, Heyd JJ, Brothers E, Kudin KN, Staroverov VN, Kobayashi R, Normand J, Raghavachari K, Rendell A, Burant JC, Iyengar SS, Tomasi J, Cossi M, Rega N, Millam JM, Klene M, Knox JE, Cross JB, Bakken V, Adamo C, Jaramillo J, Gomperts R, Stratmann RE, Yazyev O, Austin AJ, Cammi R, Pomelli C, Ochterski JW, Martin RL, Morokuma K, Zakrzewski VG, Voth GA, Salvador P, Dannenberg JJ, Dapprich S, Daniels AD, Farkas O, Foresman JB, Ortiz JV, Cioslowski J, Fox DJ (2010) Gaussian 09, revision E. Gaussian, Inc, Wallingford, p 01